JOURNAL OF GUIDANCE, CONTROL, AND DYNAMICS
Vol. 18, No. 4, July–August 1995

Dynamic Modeling of a Trailing Wire Towed by an Orbiting Aircraft

James M. Clifton*
U.S. Naval Air Warfare Center, Patuxent River, Maryland 20670
Louis V. Schmidt†
U.S. Naval Postgraduate School, Monterey, California 93943
and
Thomas D. Stuart‡
U.S. Navy, Arlington, Virginia 22202

A numerical model treating the dynamics of a long trailing wire towed by an orbiting aircraft is described. The dynamics are based on the superposition of a "dangling chain" model upon the steady-state, no-wind wire equilibrium position. Excitation is due to the wind's nonuniform vertical profile causing a once-per-orbit cycle harmonic aerodynamic input. The model was validated both by analytic methods and by comparison with experimental data.

Nomenclature

a = wire acceleration
A, B, C = convergence variables
ac = drogue aerodynamic center location, aft of leading edge
C_A = wire axial force coefficient
C_{DD} = coefficient of drag for the drogue
C_{LD} = coefficient of lift for the drogue
$C_{L\alpha D}$ = lift curve slope for the drogue
C_N = wire normal force coefficient
D = wire diameter
$D\prime$ = pseudodamping
D_D = drogue total drag force
F_a = wire aerodynamic force
F_g = wire gravitational force
F_{ID} = drogue inertial force
g = acceleration due to gravity
L = length of wire
L_D = drogue total lift force
L_1 = length of drogue
M_{LE} = moment about drogue leading edge
Q = forcing function
q = local dynamic pressure
R = radial position of wire, cylindrical coordinates
RS = superimposed radial coordinate of wire, cylindrical coordinates
S = distance along the wire
S_D = drogue maximum cross-sectional area
SF_D = drogue aerodynamic side force
T = wire tension
V = wire velocity
V_R = wire's radial velocity component, cylindrical coordinates
V_{rel} = relative velocity of wire
V_{relper} = component of V_{rel} normal of wire
V_W = wind velocity
V_θ = wire's angular velocity component, cylindrical coordinates
v = wire oscillation displacement
W_D = drogue weight
X = first orthogonal dangling chain oscillation
Y = second orthogonal dangling chain oscillation
Z = vertical position of wire, cylindrical coordinates
α = local wire angle of attack
α_D = drogue angle of attack
β_D = drogue sideslip angle
ΔS = wire segment
Δt = time step
θ = angular position of wire, cylindrical coordinates
θS = superimposed angular coordinate of wire, cylindrical coordinates
μ = weight per unit length of wire
ρ = atmospheric density
Ω = angular rotation rate of wire

Subscripts

m = time-step index
N = end gridpoint index
n = gridpoint index
r, θ, z = vector component, r, θ, or z

Superscript

$'$ = spatial derivative with respect to wire axial distance

Introduction

THERE are a number of current and proposed uses for long cables or wires towed behind ships and aircraft. For example, antisubmarine warfare ships tow long cables with embedded acoustic sensors along the cable length for the purpose of passive acoustic ranging. Knowledge of the real-time cable shape is required for the sensor process calculations.[1] Several classes of aircraft currently trail long antennas for low-frequency/long-distance communications. One proposed application[2] is to use a long cable towed by an orbiting cargo airplane to provide pinpoint airborne delivery of cargo. Wire oscillations and subsequent wire failures are problems common to many towed wire/cable applications. All of these applications share the same basic physics, which are adapted and modified to each individual case. This paper focuses upon the case of a cable and drogue system towed behind an airplane flying a constant-altitude, circular orbit.

Received June 4, 1993; presented as Paper 93-3663 at the AIAA Atmospheric Flight Mechanics Conference, Monterey, CA, August 9–11, 1993; revision received April 25, 1994; accepted for publication June 13, 1994.

*Lieutenant Commander, Aircraft Division and Force Warfare Division. Member AIAA.
†Professor Emeritus, Department of Aeronautics and Astronautics. Associate Fellow AIAA.
‡Lieutenant Commander. Member AIAA.

The analyses by Irvine and Caughey[3] for the vibrations of a Cable fixed at both ends provided much background for developing the governing equations of the towed wire. Anderson[4] extended this work and analyzed the effects of the fluid and wire interface upon the wire vibrations. Skop and Choo[2] described the equilibrium configuration of a cable towed behind a towplane flying a circular orbit, including reasons for the multivalued nature of solutions to the governing equations. A related study, an analysis by Matteis[5] into the dynamics of a sailplane when attached to a towplane, provided insight into the modeling of a drogue on the end of a wire. The studies just cited emphasized analytical solutions. Huang[6] developed a numerical model for the steady-state solution of the towed-wire problem and outlined the algebraic and differential equations required for a computer simulation of the wire in a steady-state orbit. However, his work lacked both a complete description of the numerical schemes employed and software documentation. Huang's paper formed the basis upon which the static computer simulation in this paper was developed. Crist[7] developed the first computer simulation for the dynamics of a towed wire. The problem formulation and the numerical scheme limited the wire model to very long, lumped-mass grid segments. Application of Crist's program has typically been limited to wire dynamics analysis during the reeling-in and reeling-out processes. Fidelity has been a problem when using the program in the analysis of extended-wire dynamics. Borst et al.[8] introduced the concept of fuzzy logic as a control algorithm to suppress the vertical oscillations of the towed cable's lower end during orbital motion using dynamic modeling of cable motion that included deployment, retraction, and orbiting phases of the cable system. Lawton[9] described experiments performed onboard an EC-130 TACAMO airplane to show the influence of wind shear on towed cable dynamics in both right- and left-hand orbiting flight.

Background

This paper considers the orbiting phase of towed-cable operations following reel out with the purpose of the study being to provide a reliable modeling capability for describing cable dynamics. Oscillations in the trailing wire antenna result in three critical problem areas: 1) the oscillations can cause contract between the wire and the towplane's horizontal tail, 2) oscillations in wire tension can result in failure due to exceeding the limit strength of the wire, and 3) antenna wire oscillations can cause a serious degradation in mission performance.

Verticality is defined as the altitude difference between the towplane and the drogue at the wire's lower end normalized by the length of the wire. Thus 100% verticality requires the wire to be perfectly vertical below the towplane. In a typical application, the towplane will fly a constant-altitude, circular orbit with a bank angle on the order of 20–40 deg. In this orbit, a long wire of 15,000–30,000 ft in length assumes the approximate shape of a helix with a smaller radius at the drogue than at the towplane. The wire typically makes one-half to a full turn in the helix shape from the top to the bottom. Flight test data show that vertically oscillations occur at a frequency equal to the orbit rate of the towplane. A typical period is on the order of 100–200.

Steady-State Model

The steady-state model was fundamental since its solution provided the initial condition information required by the dynamic model. The static model developed here was based on Huang's[6] governing equations. The numerical approximation of these governing equations relied on second-order-accurate central-differencing techniques. The wire was broken into a number of segments of uniform length equal to ΔS. It was assumed that 1) the shear forces were negligible and that only the tension forces were significant, 2) the wire was flying in a still, steady airmass with no winds, and 3) steady-state conditions existed with the towplane in a constant circular orbit.

Applying Newton's second law, the ordinary differential equations describing the balance of forces on an incremental section of the wire were written asin Eq. (1):

$$\frac{d\boldsymbol{T}}{dS}\Delta S + \frac{\boldsymbol{F}_a}{\Delta S}\Delta S + \frac{\boldsymbol{F}_g}{\Delta S}\Delta S = \frac{m}{\Delta S}\Delta S\frac{d\boldsymbol{V}}{dt} = \frac{m}{\Delta S}\Delta S\boldsymbol{a} \qquad (1)$$

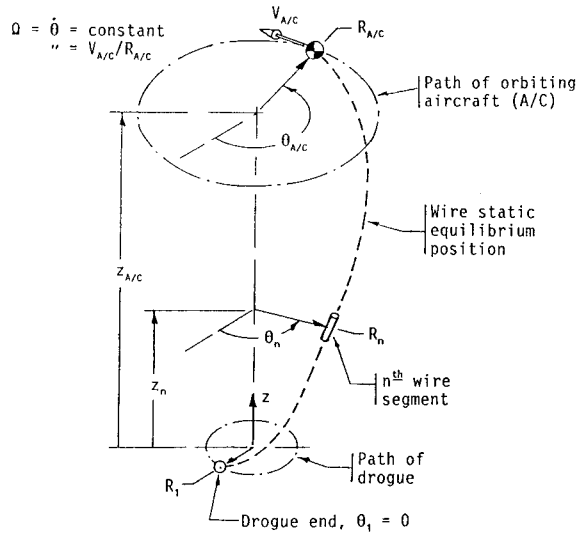

Fig. 1 Cylindrical coordinate system for static model.

Next, each term of Eq. (1) was considered individually, applying the coordinate system shown in Fig. 1. The first term in Eq. (1) was expanded about point n, Eq. (2), to yield the vector components, Eq. (3):

$$\left\{\frac{d\boldsymbol{T}}{dS}\right\}_n = \frac{\boldsymbol{T}_{n+\frac{1}{2}} - \boldsymbol{T}_{n-\frac{1}{2}}}{\Delta S}$$

$$\left\{\frac{d\boldsymbol{T}}{dS}\right\}_n = \underbrace{\{(TR')' - TR(\theta')^2\}_n \boldsymbol{e}_r}_{(2a)} \qquad (2)$$

$$+ \underbrace{\{(TR\theta')' + TR'\theta'\}_n \boldsymbol{e}_\theta}_{(2b)} + \underbrace{(TZ')'_n \boldsymbol{e}_z}_{(2c)}$$

Yielding the central-difference scalar components from Eq. (2) as

$$\text{Term(2a)} = \left\{\frac{T_{n+\frac{1}{2}}R'_{n+\frac{1}{2}} - T_{n-\frac{1}{2}}R'_{n-\frac{1}{2}}}{\Delta S}\right\}$$

Term(2b) =

$$\left\{\frac{T_{n+\frac{1}{2}}[(R_{n+1}+R_n)/2]\theta'_{n+\frac{1}{2}} - T_{n-\frac{1}{2}}[(R_n+R_{n-1})/2]\theta'_{n-\frac{1}{2}}}{\Delta S}\right\} \qquad (3)$$

$$\text{Term(2c)} = \left\{\frac{T_{n+\frac{1}{2}}Z'_{n+\frac{1}{2}} - T_{n-\frac{1}{2}}Z'_{n-\frac{1}{2}}}{\Delta S}\right\}$$

Under assumptions (2) and (3), the velocity at gridpoint n becomes the vector cross product, Eq. (4). The magnitude of the velocity is a tangential value, Eq. (5), in the $\boldsymbol{e}_\theta$ components direction since $\Omega = \dot{\theta}_n\boldsymbol{e}_z = \dot{\theta}\boldsymbol{e}_\theta = \text{const}$.

$$\boldsymbol{V}_n = \Omega \times \boldsymbol{R}_n \qquad (4)$$

$$|\boldsymbol{V}_{\text{rel}n}| = |\boldsymbol{R}_n|\dot{\theta} \qquad (5)$$

Stuart[10] provided the definitions of the wire's aerodynamic coefficients as a function of α, Eq. (6), applicable to a wire configuration that matched the available flight test data:

$$C_N = 1.09\sin^2\alpha - 0.08\sin^2(2\alpha)$$

$$C_A = \begin{cases} 0.017 & \text{for} \quad \alpha \le 45 \text{ deg} \\ 0.0 & \text{for} \quad \alpha > 45 \text{ deg} \end{cases} \qquad (6)$$

The second term in Eq. (1) at wire gridpoint n was obtained using Eq. (6) for the aerodynamics, in conjunction with the normal and

axial components of the relative velocity as obtained by a central-difference approximation; cf. Eq. (7):

$$\frac{\boldsymbol{F}_a}{\Delta S} = k_r \boldsymbol{e}_r + k_\theta \boldsymbol{e}_\theta + k_z \boldsymbol{e}_z \tag{7}$$

where

$$k_r = \tfrac{1}{2}\rho_n D(R_n\dot{\theta})^2(C_{N_n} - C_{A_n}) \times \frac{R_n(R_{n+1} - R_{n-1})(\theta_{n+1} - \theta_{n-1})}{4\Delta S^2}$$

$$k_\theta = \tfrac{1}{2}\rho_n D(R_n\dot{\theta})^2\left\{C_{N_n}\left[\frac{R_n^2(\theta_{n+1} - \theta_{n-1})^2}{4\Delta S^2} - 1\right] - C_{A_n}\frac{R_n(\theta_{n+1} - \theta_{n-1})}{2\Delta S}\right\}$$

$$k_z = \tfrac{1}{2}\rho_n D(R_n\dot{\theta})^2\left[C_{N_n}\frac{R_n(\theta_{n+1} - \theta n - 1)(z_{n+1} - z_{n-1})}{4\Delta S^2} - C_{A_n}\frac{(Z_{n+1} - Z_{n-1})}{2\Delta S}\right]$$

The third term in Eq. (1), the contribution due to the weight of the wire segment, is stated in Eq. (8):

$$\frac{\boldsymbol{F}_{\text{gn}}}{\Delta S} = -\mu g_m \boldsymbol{e}_z \tag{8}$$

The right-hand side of Eq. (1) is the inertial force acting on the wire segment and is due solely to the centrifugal force in the static case; cf. Eq. (9):

$$\frac{\boldsymbol{F}_{\text{in}}}{\Delta S} = -\mu R_n\dot{\theta}^2\boldsymbol{e}_r \tag{9}$$

Substitution of Eqs. (3) and (7–9) into Eq. (1) and rearranging yielded three equations consisting of the three orthogonal components of Eq. (1) in terms of R, θ, Z and T. The needed fourth relation, a compatibility requirement, used the definition of the unit tangent vector, Eq. (10):

$$\left(R'_{n+\frac{1}{2}}\right)^2 + \left(R_{n+\frac{1}{2}}\theta'_{n+\frac{1}{2}}\right)^2 + \left(Z'_{n+\frac{1}{2}}\right)^2 = 1 \tag{10}$$

Solution of the coupled equation set for the values at each grid-point required $T_{n+\frac{1}{2}}$, R_{n+1}, θ_{n+1}, and Z_{n+1} to be explicitly or implicitly broken out from the equations. A sufficient condition for the convergence of coupled equations using an iterative technique (c.f., Gerald and Wheatly[11] is that the sum of the partial derivatives with respect to each variable had to be less than one for each equation. This criterion was met by defining a new set of convergence variables, as shown in Eq. (11):

$$\begin{aligned} A_{n+\frac{1}{2}} &= T_{n+\frac{1}{2}}R'_{n+\frac{1}{2}} = T_{n+\frac{1}{2}}\left\{\frac{R_{n+1} - R_n}{\Delta S}\right\} \\ B_{n+\frac{1}{2}} &= T_{n+\frac{1}{2}}R_{n+\frac{1}{2}}\theta'_{n+\frac{1}{2}} \\ C_{n+\frac{1}{2}} &= T_{n+\frac{1}{2}}Z'_{n+\frac{1}{2}} \end{aligned} \tag{11}$$

where

$$A_{n+\frac{1}{2}} = A_{n-\frac{1}{2}} + R_n\left\{\frac{\left(T_{n+\frac{1}{2}} + T_{n-\frac{1}{2}}\right)(\theta_{n+1} - \theta_{n-1})^2}{8\Delta S^2} - k_r - \mu R_n\dot{\theta}^2\right\}\Delta S$$

$$B_{n+\frac{1}{2}} = B_{n-\frac{1}{2}} - \left\{\left[\frac{\left(T_{n+\frac{1}{2}} + T_{n-\frac{1}{2}}\right)(R_{n+1} - R_{n-1})(\theta_{n+1} - \theta_{n-1})}{8\Delta S^2}\right] + k_\theta\right\}\Delta S$$

$$C_{n+\frac{1}{2}} = C_{n-\frac{1}{2}} + (-k_z + \mu g)\Delta S$$

Applying the compatibility relation, Eq. (10), to Eq. (11) yields Eq. (12) for $T_{n+\frac{1}{2}}$ followed by recursion relations for the three remaining variables, Eqs. (13–15):

$$T_{n+\frac{1}{2}} = \sqrt{A^2_{n+\frac{1}{2}} + B^2_{n+\frac{1}{2}} + C^2_{n+\frac{1}{2}}} \tag{12}$$

$$R_{n+1} = R_n + \left(A_{n+\frac{1}{2}}\Delta S\right)\Big/T_{n+\frac{1}{2}} \tag{13}$$

$$\theta_{n+1} = \theta_n + \left(2B_{n+\frac{1}{2}}\Delta S\right)\Big/\left[T_{n+\frac{1}{2}}(R_{n+1} + R_n)\right] \tag{14}$$

$$Z_{n+1} = Z_n + \left(C_{n+\frac{1}{2}}\Delta S\right)\Big/T_{n+\frac{1}{2}} \tag{15}$$

The first gridpoint, $n = 1$, was defined by requiring force and moment equilibrium at the drogue attachment point. The aerodynamic coefficients for the conically shaped drogue, Eq. (16), were determined by Stuart[10]:

$$C_{DD} = 0.53$$

$$C_{LD} = \begin{cases} 0.61\alpha_D & \text{for} \quad \alpha_D < 45 \text{ deg} \\ 0.42 & \text{for} \quad 45 < \alpha_D < 60 \text{ deg} \\ 0.20 & \text{for} \quad 60 < \alpha_D < 90 \text{ deg} \end{cases} \tag{16}$$

$$ac = 0.76 \quad L_1$$

The wire tension vector, Eq. (17), at $n = 1$ becomes

$$\boldsymbol{T}_1 = (F_{ID} - SF_D)\boldsymbol{e}_r - D_D\boldsymbol{e}_\theta + (L_D - W_D)\boldsymbol{e}_z \tag{17}$$

where

$$F_{ID} = W_D\dot{\theta}^2R_1/g$$

$$SF_D = C_{L\alpha D}\beta_D q_1 S_D$$

$$D_D = C_{DD}q_1S_D$$

$$L_D = C_{L\alpha D}\alpha_D q_1 S_D$$

Under the assumptions that $T_2 = T_1$ (i.e., an implication that drogue forces dominate the first wire segment) and the T_1 tension of the first wire segment acted in the reciprocal direction to the drogue's attachment force vector, the second grid point was estimated, Eq. (18), based on an initial guess of the drogue location:

$$\begin{aligned} R_2 &= R_1 - (F_{ID} - ASFD)\Delta S/T_1 \\ \theta_2 &= \theta_1 + [2D_D\Delta S]/[T_1(R_2 + R_1)] \\ Z_2 &= Z_1 + \sqrt{\Delta S^2 - R_1^2 + 2R_2R_1\cos(\theta_2 - \theta_1) - R_2^2} \end{aligned} \tag{18}$$

The information in Eq. (18) allows a calculation of the complete, segmented wire shape using Eqs. (12–15). Since the wire's upper end would not necessarily match the aircraft's radial and vertical positions, a "shooting-the-boundary-condition" technique was used. The method consisted of updating the bottom (drogue) position by a fraction of the miss distance at the top and then iterating the recursion relations until convergence was attained.

Figures 2–6 are no-wind, static equilibrium plots of R, θ, Z, T, and α along the length of the wire for a representative flight condition corresponding to the following: Towplane airspeed = 156 KIAS (knots indicated airspeed), towplane altitude = 18,325 ft, towplane bank angle = 34 deg (assumed constant), wire length = 20,290 ft, μg = 0.0621 lb_f/in., drogue weight = 82.0 lb_f, drogue length = 2.64 ft, drogue base area = 3.14 ft^2, and drogue center of gravity = 1.15 ft from cable tie.

The wire was modeled by 200 grid segments, which was used in all subsequent analysis. It will be noted on Figs. 3–5 that the plots of θ, Z, and T along the wire length approached a linear variation. The wire tension at the towplane, shown on Fig. 5, was 930 lb, which is less than the total dead weight of the wire and drogue (1342 lb), mainly due to the aerodynamic forces acting on the wire. Figure 6

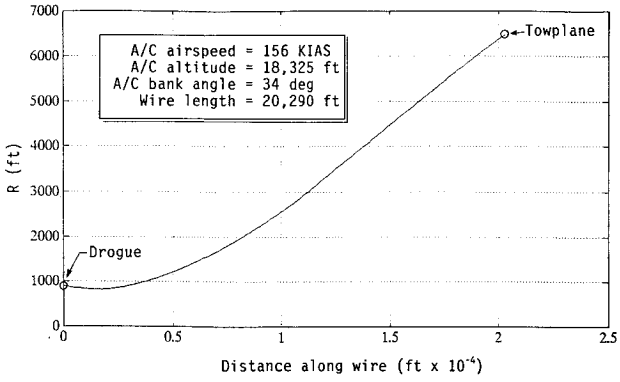

Fig. 2 Radial R coordinate variation along wire.

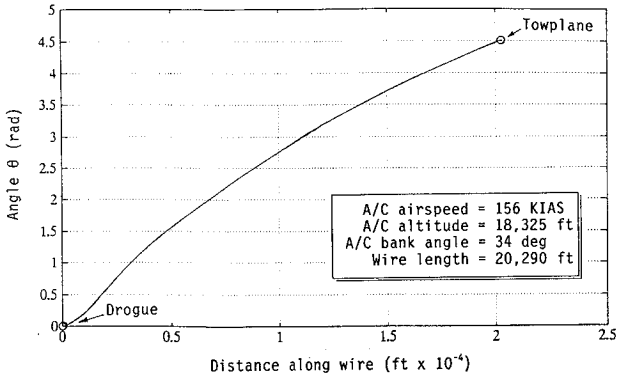

Fig. 3 Angular θ coordinate variation along wire.

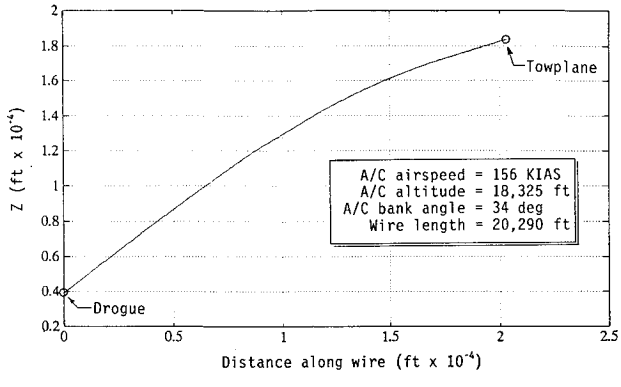

Fig. 4 Vertical z coordinate variation along wire.

shows that the true wire angle of attack increased from a low value at the towplane to near vertical at the lower end.

Validation of the method included 1) using the aerodynamic coefficients and physical parameters of Huang[6] (good agreement was found), 2) trailing a massless wire and drogue straight back from the towplane at very low towplane back angles, and 3) zeroing of the aerodynamic coefficients that resulted in a wire verticality value of 1.0 at low towplane bank angles.

Dynamic Model

The dynamic model was developed under several assumptions:

1) All displacements from the steady-state equilibrium condition were small and normal to the wire's static position.

2) The towplane flew a constant circular orbit.

3) The dangling chain modeled all significant wire dynamics.

4) Wire torsion, stretching, and bending effects were insignificant.

5) The steady-state tension distribution was used in the dynamic model.

The governing partial differential equation for a dangling chain having boundary conditions (B.C.) of one end fixed and the other end as free with a concentrated mass was solved by Clifton.[12] The independent variable $v(S, t)$ in Eq. (19) represents the displacement from the static equilibrium position due to the dangling chain motion. The coordinate system used in the dynamic model was referenced from the top (at the towplane) to the bottom (at the drogue), which is opposite to the steady-state model. The forcing function $Q(S, t)$ was defined as acting normal to the wire at any grid point with dimensions of force per unit length. The initial conditions (I.C.) were the static position with zero displacement rate. This assumption led to a short starting transient at the beginning of the dynamic model simulation. Two separate, orthogonal solutions to Eq. (19) were required to model the two-dimensional displacement of each grid point about the equilibrium position:

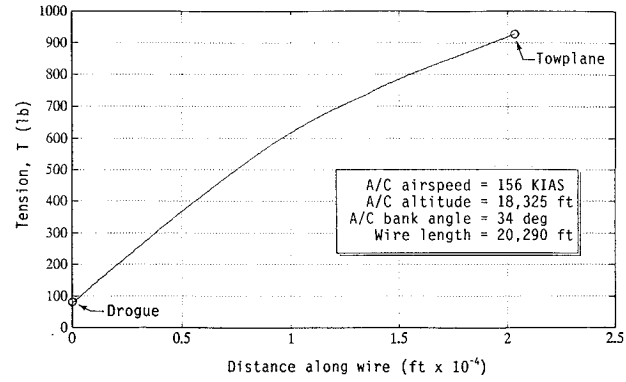

Fig. 5 Variation of tension T along wire.

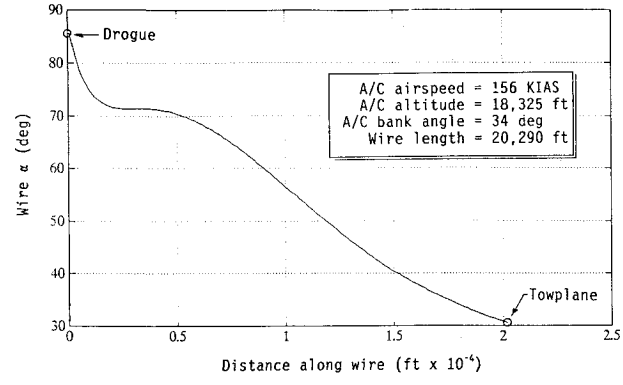

Fig. 6 True α variation along wire.

$$\mu \frac{\partial^2 v(S, t)}{\partial t^2} = \frac{\partial}{\partial S}\left\{T(S)\frac{\partial v(S, t)}{\partial S}\right\} + Q(S, t) \qquad (19)$$

B.C.: $v(0, t) = 0$ and $v(L, t) \Rightarrow$ bounded

$$T(L)\frac{\partial v(L, t)}{\partial S} + Q(L, t) = \left(\frac{W_D}{g}\right)\frac{\partial^2 v(L, t)}{\partial t^2}$$

I.C. $v(S, 0) = f(S)$ and $\partial v/\partial t(S, 0) = 0$.

Equation (19) was approximated by a second-order-accurate central-difference scheme, Eq. (20), using n as the spatial grid-point number index starting from the wire's upper end, m as the time step index, and $T(n) = T_n$ = the steady-state tension distribution. The forcing function was defined as $Q_{n,m}$, with the indices at n, m. Since T_n was a constant over time, the expression Eq. (20) was explicit in the variable $v_{n,m+1}$. It was then possible to envision a fully explicit marching scheme requiring knowledge only of the two end gridpoints and the two previous time-step solutions:

$$\mu\left\{\frac{v_{n,m+1} - 2v_{n,m} + v_{n,m-1}}{\Delta t^2}\right\}$$

$$= \left\{\frac{T_{n+\frac{1}{2}}(v_{n+1,m} - v_{n,m}) - T_{n-\frac{1}{2}}(v_{n,m} - v_{n-1,m})}{\Delta S^2}\right\} + Q_{n,m} \qquad (20)$$

The first two boundary conditions of Eq. (19) imply that the wire is pinned at the top and the displacement is bounded at the bottom. The third boundary condition ensured force equilibrium at the drogue position, $n = N$, and may be expressed in a central-difference form, Eq. (21):

$$T_N\left\{\frac{v_{N-1,m} - v_{N+1,m}}{2\Delta S}\right\} + Q_{N,m} = \frac{W_D}{g}\left\{\frac{v_{N,m+1} - 2v_{N,m} + v_{N,m-1}}{\Delta t^2}\right\} \tag{21}$$

Equation (21) described the balance between the tension and forcing function forces and the lateral acceleration of the drogue (remember that all motion was defined as lateral in the dangling chain problem). It was next assumed that the forces acting on the drogue were much greater than the forces on the last segment of wire. Later analyses showed that the forces differed by two orders of magnitude. Based on this assumption, it was further assumed that the wire slope was nearly constant at the drogue attachment point and the shape of the wire was determined by the drogue forces and not the distributed wire forces. This condition was approximated by defining an artificial $(N+1)$ point beyond the drogue followed by a central-difference approximation to equate the slope at the half-step before and after the drogue, Eq. (22):

$$\frac{v_{N,m} - v_{N-1,m}}{\Delta S} = \frac{v_{N+1,m} - v_{N,m}}{\Delta S} \tag{22}$$

Under the assumption that the forces on the drogue were much greater than on the adjacent wire segment, one can express $T_N = T_{N-1} = T_{N-\frac{1}{2}}$. Using this assumption combined with solving Eq. (22) for $v_{N+1,m}$ allows the determination of $v_{n,m+1}$ from Eq. (21) in terms of previously known quantities yielding Eq. (23):

$$v_{N,m+1} = \frac{\Delta t^2 g}{W_D}\left[T_{N-\frac{1}{2}}\left\{\frac{v_{N-1,m} - v_{N,m}}{\Delta S}\right\} + Q_{N,m}\right] + 2v_{N,m} - v_{N,m-1} \tag{23}$$

In applying the wind as a forcing function, it was important to first note that, for the assumed steady-state angle of bank turn, the towplane moved with the airmass. This observation implies that the wind derived forcing function was zero at the towplane. The required apparent wind-forcing function was obtained by adding the negative of the wind vector at the towplane station to the winds at each gridpoint of the wire.

The term $Q_{N,m}$ was derived from the apparent forcing wind. Since the forcing function was defined perpendicular to the wire, only that component of the apparent forcing wind normal to the wire was used to determine the forcing function. The orientation of the forcing function with the wire varied harmonically as the wire orbited within the airmass. Calculations were made for each orthogonal component of the oscillation yielding one component that varied harmonically as a sine function whereas the second varied as a cosine function. Two adjustments in phasing were required for the harmonic functions. The first phase correction was the θ coordinate at each gridpoint to account for the fact that at every gridpoint except the towplane's, the wire shape had to rotate through the angle θ for $\boldsymbol{e}_\theta$ to be aligned with the 000-deg heading. The second phase correction accounted for the wind heading at each gridpoint generally being different from 000 deg. Finally, the aerodynamic coefficients of the wire were used to convert the forcing wind term into a force vector, which was the true wind generated forcing function. The forcing function relations are provided by Eq. (24) with the radial and tangential velocity components described by Eq. (25):

$$\begin{aligned} Q_r(x)\boldsymbol{e}_r &= V_{\mathrm{rn}} \sin(\dot{\theta}t - \theta')\boldsymbol{e}_r \\ Q_\theta(x)\boldsymbol{e}_\theta &= V_{\theta n} \cos(\dot{\theta}t - \theta')\boldsymbol{e}_\theta \end{aligned} \tag{24}$$

where $\theta' = \theta - \theta_w$

$$V_{\mathrm{rn}} = A_n\sqrt{a_n^2 + b_n^2 + c_n^2}, \qquad V_{\theta n} = A_n\sqrt{a_n^2 + b_n^2 + e_n^2} \tag{25}$$

where

$$A_n = \tfrac{1}{2}\rho_n V_{wn}^2 DC_N$$

$$a_n = \frac{R_n(R_{n+1} - R_{n-1})(\theta_{n+1} - \theta_{n-1})}{4\Delta S^2}$$

$$b_n = 1 - \frac{(R_{n+1} - R_{n-1})^2}{4\Delta S^2}$$

$$c_n = \frac{(R_{n+1} - R_{N-1})(Z_{n+1} - Z_{n-1})}{4\Delta S^2}$$

$$d_n = 1 - \frac{[R_n(\theta_{n+1} - \theta_{n-1})]^2}{4\Delta S^2}$$

$$e_n = \frac{R_n(\theta_{n+1} - \theta_{n-1})(Z_{n+1} - Z_{n-1})}{4\Delta S^2}$$

The next task was to derive the algorithm to superimpose $X_{n,m}$ and $Y_{n,m}$, the orthogonal components of the dangling chain oscillation, onto the steady-state solution. The $X_{n,m}$ and $Y_{n,m}$ displacement components were defined as being in the $\boldsymbol{e}_r$, $\boldsymbol{e}_\theta$ plane and thus orthogonal to the $\boldsymbol{e}_z$ vector. Next, the governing relation for the dangling chain, Eq. (19), was derived assuming that the displacements were normal to the chain. This implied that the $X_{n,m}$ and $Y_{n,m}$ displacements were orthogonal to the unit tangent vector at each gridpoint. The cross product of the $\boldsymbol{e}_z$ with the unit tangent vector in cylindrical coordinates then defined the direction of the $X_{n,m}$ displacement component in the cylindrical coordinate system used for the superimposed model. The $Y_{n,m}$ displacement component was orthogonal to the unit tangent vector and the $X_{n,m}$ displacement. The direction of the $Y_{n,m}$ displacement in cylindrical coordinates was obtained using the cross product of the vector in the direction of the $X_{n,m}$ displacement and the unit tangent vector at each gridpoint. The $\boldsymbol{e}_r$ and $\boldsymbol{e}_\theta$ displacement components were added to the R_n and θ_n coordinates of the steady-state gridpoint locations to derive the time-dependent superimposed locations $RS_{n,m}$ and $\theta S_{n,m}$. The superposition relations are given by Eqs. (26) and (27). The time-dependent, superimposed $ZS_{n,m}$ location was obtained using compatibility relations derived from the known length of ΔS for the first internal gridpoint and the definition of the unit tangent vector for all subsequent gridpoints:

$$RS_{n,m} = R_n + X_{n,m}\left\{\frac{R_n(\theta_{n+1} - \theta_{n-1})}{2f_n\Delta S}\right\} + Y_{n,m}\left\{\frac{(R_{n+1} - R_{n-1})(Z_{n+1} - Z_{n-1})}{4f_n\Delta S^2}\right\} \tag{26}$$

$$\theta S_{n,m} = \theta_n + X_{n,m}\left\{\frac{(R_{n+1} - R_{n-1})}{2R_n f_n\Delta S}\right\} - Y_{n,m}\left\{\frac{(\theta_{n+1} - \theta_{n-1})(Z_{n+1} - Z_{n-1})}{4f_n\Delta S^2}\right\} \tag{27}$$

where

$$f_n = \sqrt{\frac{(R_{n+1} - R_{n-1})^2 + R_n^2(\theta_{n+1} - \theta_{n-1})^2}{4\Delta S^2}}$$

Two forms of pseudodamping were modeled. The first was due to the drag increment caused by the lateral oscillation rate. It was assumed that the small displacement, lateral oscillations remained perpendicular to the wire's steady-state positions, which implied that the drag behaved similarly. The drag force was thus always orthogonal to the steady-state wire shape and opposite in direction to the lateral velocity of the wire gridpoints. This was because the lateral oscillations were calculated based on the assumption that they remained orthogonal to the steady-state wire. The central-difference approximation for the contribution to the total pseudodamping from the lateral oscillation rate is given by Eq. (28):

$$D'_{n,m} = C_N D \tfrac{1}{2}\rho_n \left(\frac{v_{n,m+1} - v_{n,m-1}}{2\Delta t}\right)\left|\left(\frac{v_{n,m+1} - v_{n,m-1}}{2\Delta t}\right)\right| \tag{28}$$

Note that $v_{n,m+1}$ was required to determine $D'_{n,m}$; $D'_{n,m}$ was also required in the calculation of $v_{n,m+1}$, which necessitated an iteration at each gridpoint for the new position in time. This pseudodamping force dominated when the rate was highest and usually occurred as the wire was passing through the initial static equilibrium position.

The next task was to consider the restorative for due to the change in angle of attack of the wire in the displaced position. On the average, as the wire moved above equilibrium, the angle of attack reduced, and conversely, on the average, as the wire moved below the equilibrium position, the angle of attack increased. For this reason, angle of attack effects were restorative during oscillations. The term α_n was defined as the steady-state angle of attack, $\alpha S_{n,m}$ was defined as the displaced angle of attack, and $\Delta\alpha_{n,m}$ was the difference between the two angles. The finite difference approximation for the two angles is stated in Eq. (29):

$$\alpha_n = \arccos\left\{\frac{R_n(\theta_{n-1} - \theta_{n+1})}{2\Delta S}\right\}$$

$$\alpha S_{n,m} = \arccos\left\{\frac{RS_{n,m}(\theta S_{n-1,m} - \theta S_{n+1,m})}{2\Delta S}\right\} \tag{29}$$

The change of relative perpendicular velocity in the displaced geometry, $\Delta V_{\text{relper}\,n,m}$, defined by Eq. (30), provides the final value for $D'_{n,m}$, Eq. (31):

$$\Delta V_{\text{relper}\,n,m} = R_n\dot{\theta}\sin(\Delta\alpha_{n,m}) \tag{30}$$

$$D'_{n,m} = C_N D\tfrac{1}{2}\rho_n(\Delta V_{\text{relper}\,n,m})|(\Delta V_{\text{relper}\,n,m})| \tag{31}$$

The restorative force, Eq. (31), was resolved into components that were applied to the calculations of $X_{n,m}$ and $Y_{n,m}$, Eq. (32). All calculations for pseudodrag due to angle of attack changes were in terms of time step m, and so this force was determined at time $m+1$ without resorting to an iterative scheme:

$$D'_{Xn,m} = \frac{|X_{n,m}|D'_{n,m}}{\sqrt{X^2_{n,m} + Y^2_{n,m}}}$$

$$D'_{Yn,m} = \frac{|Y_{n,m}|D'_{n,m}}{\sqrt{X^2_{n,m} + Y^2_{n,m}}} \tag{32}$$

Von Neumann's stability analysis was considered for the dangling chain problem with results as shown in Eq. (33). A 200-segment grid pattern was chosen with a $\Delta t = 0.1$ s. The most restrictive case was for a wire of the smallest reasonable length and the corresponding largest tension value. The criterion was met for these extreme conditions:

$$\frac{\Delta t^2 T}{\Delta S^2 \mu} \leq 1 \tag{33}$$

The dynamic simulation program required a number of data files that were generated by the steady-state program. As implemented, the dynamic program used the 200-segment spatial grid and the 10th of a second time step size selected earlier. The program ran at about 1.3 real time on a 486-33 MHz desktop computer. Program outputs included $X_{n,m}$ and $Y_{n,m}$ displacement snapshots and time history plots of verticality, towpoint tension, drogue position, and the wire position 45 ft aft of the towpoint.

Validation of the dangling chain portion of the model was performed by comparing the program's two-dimensional displacement results with the analytical solution of a dangling chain without a concentrated mass on the wire's end. The homogeneous response of the dangling chain model matched the eigenvector and eigenvalue for an initial displacement condition of that eigenvector, thereby validating the simulation code.

Examination of the $X_{n,m}$ and $Y_{n,m}$ displacements at various times disclosed that the wire had, at most, three slope reversals and the changes were fairly gentle. As seen in Eqs. (20) and (21), the first and second partial derivatives used in the dangling chain simulation were approximated using a central-differencing technique. Applying the method of Gerald and Wheatley,[11] the error for the central-difference approximations of the dangling chain derivatives were calculated at each gridpoint for a representative example and then averaged over each gridpoint. The resulting average truncation errors as a percentage of the calculated derivatives were shown to be less than 0.1%.

The dynamic model was run using a 0.1-s time step and a 200-point spatial grid and compared with a model having a 0.05-s time step and a 400-point spatial grid. The outputs were essentially identical, validating the choice of spatial and time grids.

As noted previously, the steady-state tension distribution was used vice the fully time-dependent tension distribution in the dangling chain displacement calculations. The fully time-dependent tension value, $T(S,t) = T(S) + \Delta T(S,t)$, was considered in Eq. (19) for a representative case. The order of magnitude of each resulting term was calculated by averaging the absolute value of each term along the entire wire length at a single point in time. The truncated terms, which contained ΔT, were at least an order of magnitude smaller than the retained terms. Little error was introduced by using the time-independent tension distribution.

The dynamic model assumed that the towplane flew a constant-altitude, circular orbit, which implied that transients in towplane pitch, bank, and yaw attitudes were ignored. This assumption was based on the observation that on days when the winds were calm at all altitudes along the wire and the crew was flying a normal mission profile, the wire maintained a constant shape without oscillations occurring in verticality or towpoint tension. Consequently, slight normal aircraft maneuvering transients were considered as insignificant.

The dynamic model also assumed that wire bending, torsion, and stretching effects did not contribute to the wire oscillations. Wire bending influences were considered insignificant since it was estimated that the maximum length of a cantilevered wire segment that could support its own weight with at most a deflection of 10% of the segment length was approximately 3 ft. The axial wavespeed (a function of axial stiffness) for a representative wire was estimated at 11,000 ft/s, which implied that tension waves in a 20,000-ft-long wire would propagate the wire's length in approximately 2 s. This propagation period was two orders of magnitude less than the orbit period of the towplane and the period of the wire oscillation and therefore was considered as a negligible influence. A similar estimate for the torsional wavespeed was 6800 ft/s, which would propagate along 20,000 ft of wire in approximately 3 s. Additionally, the drogue on the free end of the wire was typically axisymmetric, allowing torsion disturbances to merely cause a rotation of the drogue. It was assumed that the torsion waves would, in the worst case, result in drogue rotation that would dissipate before contributing to the wire dynamics.

The dynamic model was run using a wind profile of zero along the entire wire length except at the three gridpoints located at the wire's midlength. The simulation was run for wind velocity values from zero to 200 kn. After the startup transient had occurred, the oscillations were symmetric about the steady-state wire and drogue positions for all but the very large wind inputs. The model was divergent at the 200-kn wind velocity. The application of superposition required that the mean oscillation value remain close to the steady-state value for results to be valid. As the oscillation magnitude approached the region where divergence occurred, the mean radius began to depart from the steady-state value. For verticality oscillations of less than 20%, the mean radius shifted from the steady-state value less than 0.5%. For all conditions tested, the superposition of the dangling chain vibrations on the steady-state model was valid and resulted in a nondivergent simulation for verticality oscillations of less than 20%.

As a final check of the fidelity of the static and dynamic models, the simulation output was compared with flight-test data taken June 1, 1991, during E-6A TACAMO flight number 27-05 using the same flight and atmospheric conditions. Radiosonde readings were available to define the atmospheric conditions. The static equilibrium plots, Figs. 2–6, were evaluated for the same flight conditions and formed the basis for the modeling results shown in Fig. 7. In

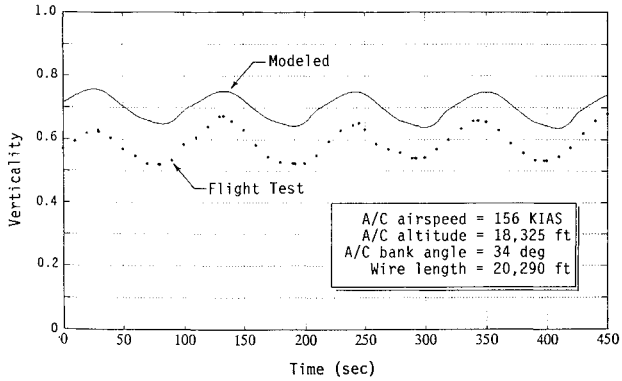

Fig. 7 Wire verticality comparison between flight test and modeled time histories.

Fig. 7, the solid line is a plot of the simulated verticality time history whereas the starred symbols represent flight-test data. The difference between the modeled and the experimentally measured verticality was approximately 8%. More importantly, the magnitude of the oscillation, frequency, and phasing correlated.

Concluding Remarks

The technique of superimposing the dynamics based on the classical dangling chain equation onto the steady-state solution of the long wire towed behind an aircraft has been validated for a wide range of forcing functions and flight conditions. The numerical code was checked against a number of analytical solutions, and the final results showed excellent correlation to flight-test derived data.

References

[1]Payne, C. M., "Parameterization of a Linear Array During Ship Maneuvers," Master's Thesis, Dept. of Mechanical Engineering, Naval Postgraduate School, Monterey, CA, March 1992.

[2]Skop, R. A., and Choo, Y., "The Configuration of a Cable Towed in a Circular Path," *Journal of Aircraft*, Vol. 8, No. 11, 1971, pp. 856–862.

[3]Irvine, H. M., and Caughey, T. K., "The Linear Theory of a Suspended Cable," *Proceedings of the Royal Society of London*, Vol. 341A, March 1974, pp. 299–315.

[4]Anderson, W. J., "Dynamic Instability of a Cable in Incompressible Flow," AIAA Paper 73-395, March 1973.

[5]Matteis, G., "Dynamics of a Towed Sailplane," AIAA Paper 91-2862, Aug. 1991.

[6]Huang, S. L., "Mathematical Model for a Long Cable Towed by Orbiting Aircraft," U.S. Naval Air Development Center, NADC-AM-6849, Warminster, PA, June 1969.

[7]Crist, S. A., "Analysis of the Motion of a Long Wire Towed from an Orbiting Aircraft," *The Shock and Vibration Bulletin*, Bulletin 41, Pt. 6, Dec. 1970, pp. 61–73.

[8]Borst, R. G., Greisz, G. F., and Quynn, A. G., "Fuzzy Logic Control Algorithm for Suppressing E-6A Long Trailing Wire Antenna Wind Shear Induced Oscillations," AIAA Paper 93-3868, Aug. 1993.

[9]Lawton, J. G., "TACAMO Flight Investigations," Cornell Aeronautical Lab., Rept. JC5039-B-2, Buffalo, NY, June 1972.

[10]Stuart, T. D., "Experimental Study of the Effect of Helical Grooves on Infinite Cylinders," Engineer's Thesis, Dept. of Aeronautics and Astronautics, Naval Postgraduate School, Monterey, CA, Dec. 1992, pp. 66, 67; see also AIAA Paper 93-3456, Aug. 1993.

[11]Gerald, C. F., and Wheatley, P. O., *Applied Numerical Analysis*, 4th ed., Addison–Wesley, Reading, MA, 1990.

[12]Clifton, J. M., "Modeling and Control of a Trailing Wire Towed by an Orbiting Aircraft," Ph.D. Thesis, Dept. of Aeronautics and Astronautics, Naval Postgraduate School, Monterey, CA, Sept. 1992.